THE JOURNAL OF PHYSICAL CHEMISTRY C

Article

Cite This: J. Phys. Chem. C 2019, 123, 29155−29161

pubs.acs.org/JPCC

# Crystal Engineering of $Bi_2WO_6$ to Polar Aurivillius-Phase Oxyhalides

Kazuki Morita,*[,†,‡] Ji-Sang Park,[§] Sunghyun Kim,[‡] Kenji Yasuoka,[†] and Aron Walsh*[,‡,∥]

[†]Department of Mechanical Engineering, Keio University, Yokohama 223-8522, Japan

[‡]Department of Materials, Imperial College London, London SW7 2AZ, United Kingdom

[§]Department of Physics, Kyungpook National University, Daegu 41566, Korea

[∥]Department of Materials Science and Engineering, Yonsei University, Seoul 03722, Korea

Supporting Information

**ABSTRACT:** The Aurivillius phases of complex bismuth oxides have attracted considerable attention because of their lattice polarization (ferroelectricity) and photocatalytic activity. We report a first-principles exploration of $Bi_2WO_6$ and the crystal engineering through replacing $W^{6+}$ by pentavalent ($Nb^{5+}$ and $Ta^{5+}$) and tetravalent ($Ti^{4+}$ and $Sn^{4+}$) ions, with charge neutrality maintained by the formation of a mixed anion oxyhalide sublattice. We find that $Bi_2SnO_4F_2$ is thermodynamically unstable, in contrast to $Bi_2TaO_5F$, $Bi_2NbO_5F$, and $Bi_2TiO_4F_2$. The electric dipoles introduced by chemical substitutions in the parent compound are found to suppress the spontaneous polarization from 61.55 $\mu C/cm^2$ to below 15.50 $\mu C/cm^2$. Analysis of the trends in electronic structure, surface structure, and ionization potentials is reported. This family of materials can be further extended with control of layer thicknesses and choice of compensating halide species.

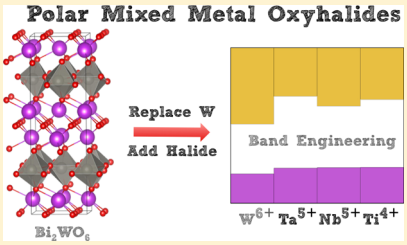


## INTRODUCTION

Metal oxides have been studied intensively for applications such as photoelectrochemistry, photocatalysis, and transparent electronics.[1−4] These studies are motivated by their low cost, high stability, and a wide range of physical properties.[3,5,6] For photochemical and optoelectronic applications, specific band gaps and band alignments are required to optimize the device performance. Many metal oxides have a valence band maximum (VBM) composed of O 2p orbitals, resulting in similar valence band energies.[7] Therefore, metal oxides often fail to meet the band alignment requirements. The most prominent example is when metal oxides are used as photoanodes for water splitting, where the valence band energy is too deep to efficiently support oxygen evolution reactions.[5,8] For the reaction to occur efficiently, the valence band edge must be higher in energy (closer to vacuum) so that holes can be effectively transferred to water. The valence band energy is relevant to other application areas including p-type transparent electrodes.[4,9]

Efforts to modulate the valence band energy of metal oxides include the use of $ns^2$ post-transitional metal cations and mixed anions.[10−13] There are few examples where these approaches are used in tandem, and there have been some notable successes.[12] The combination of high-throughput materials screening and experimental synthesis reported a p-type transparent conducting oxide $Ba_2BiTaO_6$, where high hole mobility was attributed to the hybridization of Bi 6s and O 2p levels.[14] Other experimental works have demonstrated that compounds in Sillen−Aurivillius phase, $Bi_4NbO_8X$ (where X = Cl, Br, and I), exhibit an elevated valence band.[15−17] The ability of halide anions to change the strength of an O-cation bond and hybridization of Bi with O 2p levels combine to raise the VBM compared to conventional metal oxides.[12,13] These studies suggest effectiveness of adopting mixed anion ternary and quaternary bismuth oxides to obtain elevated valence band energies. In particular, the chemical flexibility of Aurivillius-phase compounds is expected to be suitable for this approach.[18]

The general formula of the Aurivillius family is $(Bi_2O_2)^{2+}(A_{m-1}B_mO_{3m+1})^{2-}$.[18−21] Much effort has been put into studying russellite $Bi_2WO_6$ ($m$ = 1), a naturally occurring mineral, which exhibits high catalytic performance and ion conductivity.[22−24] However, because of its chemical and structural complexity, even in the simplest case of $Bi_2WO_6$, there is still much to be explored. Early in the research of this compound, several crystal structure models were proposed.[25,26] However, it is now generally accepted that $Bi_2WO_6$ adopts a polar $P2_1ab$ space group at low and intermediate temperatures.[27−29] Above 700 °C, the structure transforms into an orthorhombic $Aba2$ space group through a second-order phase transition.[27,30,31] Further heating to about 950 °C transforms the crystal to the $A2/m$ symmetry through a first-order phase transition, where the spontaneous polarization disappears ($T_C$ = 950 °C).[27,31,32]

Along with experiments, density functional theory (DFT) calculations have been used to probe the mechanism behind the structural phase transition of $Bi_2WO_6$.[31,33] Recently, researchers have expanded the scope to quaternary mixed anion compounds such as $Bi_2TaO_5F$, $Bi_2NbO_5F$, and $Bi_2TiO_4F_2$, and the photocatalytic performance of these

Received: October 18, 2019
Revised: November 7, 2019
Published: November 8, 2019






DOI: 10.1021/acs.jpcc.9b09806
J. Phys. Chem. C 2019, 123, 29155−29161

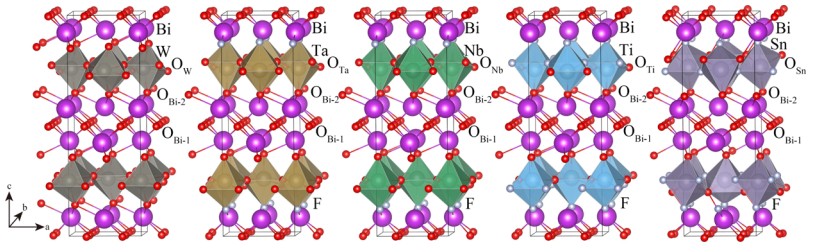


**Figure 1.** Crystal structures of $Bi_2WO_6$, $Bi_2TaO_5F$, $Bi_2NbO_5F$, $Bi_2TiO_4F_2$, and $Bi_2SnO_4F_2$. Oxygen sites are distinguished as $O_{Bi-1}$, $O_{Bi-2}$, $O_W$, $O_{Ta}$, $O_{Nb}$, $O_{Ti}$, and $O_{Sn}$.

compounds were measured.[34−36] These studies have shown the effectiveness of crystal engineering, realized through the B-site cation replacement and F addition, to make a mixed anion compound. Although the application potential of quaternary compounds was demonstrated,[34−41] less is known about their physical properties and electronic characteristics.

In this study, we systematically expand the crystal system by replacing $W^{6+}$ in $Bi_2WO_6$ with pentavalent $Ta^{5+}$ and $Nb^{5+}$ and with tetravalent $Ti^{4+}$ and $Sn^{4+}$. $F^-$ were also incorporated to the $O^{2-}$ site resulting in the charge neutrality to be maintained. Therefore, we have explored properties of a ternary compound $Bi_2WO_6$ and quaternary compounds $Bi_2TaO_5F$, $Bi_2NbO_5F$, $Bi_2TiO_4F_2$, and $Bi_2SnO_4F_2$ in detail using first-principles material modeling. We report that substitution of O with F resulted in a modified perovskite-like $(BO_4)^{2-}$ layer, which suppressed the magnitude of the spontaneous electric polarization. Furthermore, the quaternary compounds exhibited higher valence band energy compared to $Bi_2WO_6$, and each of the conduction band minimum levels differed largely, suggesting high tunability of the band edge energy. Together, these results demonstrate the diverse material properties of $Bi_2WO_6$-based compounds and open up a path toward developing new Bi-based mixed anion compounds.

## METHODS

**Atomic Structure Models.** A crystal structure model of $Bi_2WO_6$ was obtained by optimizing the initial (room temperature) structure determined from X-ray diffraction.[42]

B-site cations, W, in $Bi_2WO_6$ were replaced by Nb, Ta, Ti, and Sn, together with F, to maintain the same valence electron count, resulting in $Bi_2TaO_5F$, $Bi_2NbO_5F$, $Bi_2TiO_4F_2$, and $Bi_2SnO_4F_2$, respectively (Figure 1). Because there are degrees of freedom for the F distribution among the anion sites, 20 different F configurations were considered for each compound. Within the 20 configurations, 5 were chosen so that F atoms are aligned in a certain crystal plane and the rest were randomly selected using the site-occupancy disorder code.[43] To validate the dependence of F configurations, four most stable F configurations were calculated for each quaternary oxide. However, F configurations had little effect on the properties of interest; therefore, only the results of the most stable structures are presented.

To assess the thermodynamic stability of the Aurivillius-phase compounds, a number of decomposition reactions were considered. When the product (secondary phases) has lower energy, the reaction is exothermic, thus suggesting the quaternary compound to be unstable over any chemical potential range.

**DFT Calculations.** DFT calculations were performed within the projector-augmented wave scheme as implemented in VASP.[44−46] The VESTA[47] package was used to visualize the atomic structures. Both HSE06[48] and PBEsol[49] were used for the exchange correlation functional as described below. Scalar relativistic corrections are included in all cases. Because the valence band edges were composed of Bi 6s and O 2p orbitals, the spin−orbit coupling (SOC) effect is expected to be small and would only affect the empty Bi 6p band.[50,51]

The structure relaxations were performed using PBEsol, while further electronic structure and total energy analysis was performed with HSE06. A plane wave cutoff of 550 eV, a *k*-point sampling of at least 5 × 5 × 2 for the primitive unit cell of 36 atoms, and an electronic convergence criteria of $10^{-8}$ eV were employed. The lattice constants and the internal coordinates were optimized until the residual force became less than 1.0 meV/Å for each atom in the unit cell.

**Spontaneous Lattice Polarization.** Lattice polarization was calculated with the PBEsol functional within the Berry phase formalism.[52,53] In modern theory of polarization, the spontaneous polarization $\Delta p$ is defined as follows

$$\Delta p = P_{\text{polar}} - P_{\text{non-polar}} + n\Delta P_Q \quad (1)$$

Here, $P_{\text{polar}}$ is the *formal* polarization of the polar phase, $P_{\text{non-polar}}$ is the *formal* polarization of the nonpolar phase, $n$ is an integer, and $\Delta P_Q$ is a polarization quanta. The two *formal* polarizations are the raw results of the Berry phase calculations and the spontaneous polarization $\Delta p$ is defined as their difference.[52,53]

This definition leaves an ambiguity in the value of spontaneous polarization $\Delta p$ with respect to modulo $\Delta P_Q$, which is not a problem when $\Delta P_Q$ is larger than $\Delta p$. However, the polarization quanta $\Delta P_Q$ in Aurivillius-phase compounds was smaller than the spontaneous polarization $\Delta p$ (Table 1),

**Table 1. Structure, Polarization Quanta ($\Delta P_Q$), and Spontaneous Polarization ($\Delta p$) of Aurivillius-Phase Oxides**

| compound | *a* (Å) | *b* (Å) | *c* (Å) | volume (Å$^3$) | $\Delta P_Q$ ($\mu$C/cm$^2$) | $\Delta p$ ($\mu$C/cm$^2$) |
|---|---|---|---|---|---|---|
| $Bi_2WO_6$ | 5.44 | 5.44 | 16.55 | 489.66 | 17.79 | 61.55 |
| $Bi_2TaO_5F$ | 5.40 | 5.41 | 16.58 | 484.26 | 17.87 | 10.68 |
| $Bi_2NbO_5F$ | 5.39 | 5.40 | 16.58 | 482.08 | 17.90 | 15.50 |
| $Bi_2TiO_4F_2$ | 5.36 | 5.38 | 16.30 | 470.15 | 18.26 | 15.15 |
| $Bi_2SnO_4F_2$ | 5.53 | 5.53 | 16.83 | 515.02 | | |

making it difficult to determine the exact value of spontaneous polarization $\Delta p$ from only $P_{\text{polar}}$ and $P_{\text{non-polar}}$. Therefore, *formal* polarization of the intermediate structures between the ideal (fictitious) nonpolar centrosymmetric structure and the polar $P2_1ab$ structure were calculated. Because spontaneous polarization has some dependence on F configurations in the oxyhalide systems, the four most stable F configurations were calculated for each of the quaternary compounds.



DOI: 10.1021/acs.jpcc.9b09806
J. Phys. Chem. C 2019, 123, 29155−29161

**Surface Structure and Stability.** To find the favored crystal terminations, the atomic chemical potentials were used to obtain the surface formation energies. First, the set of chemical potentials which stabilize $Bi_2WO_6$ were obtained by comparing the formation enthalpy with the competing binary oxides, $WO_2$, $WO_3$, and $Bi_2O_3$. The formation enthalpy was calculated as follows

$$\Delta H_f^{Bi_2WO_6} = E_{Bi_2WO_6} - 2E_{Bi} - E_W - 6E_O \quad (2)$$

where $E_{Bi}$, $E_W$, and $E_O$ are the energies per atom for the standard state of elements such as Bi metal, W metal, and molecular $O_2$, respectively. To stabilize the material, the chemical potential with respect to the standard states of Bi, W, and O should satisfy the following inequality

$$\Delta H_f^{Bi_2WO_6} = \Delta\mu_{Bi_2WO_6} - 2\Delta\mu_{Bi} - \Delta\mu_W - 6\Delta\mu_O \quad (3)$$

$$\Delta\mu_{Bi} \le 0,\ \Delta\mu_W \le 0,\ \Delta\mu_O \le 0 \quad (4)$$

Second, surface formation energies $\Delta E_{surf}^f$ for given chemical potentials were calculated. Accounting for the fact that $Bi_2WO_6$ is likely to exhibit surfaces on the [001] direction,[54,55] five different models with (001) surface terminations were considered.

Surfaces were described using symmetric slab models with a thickness of at least 32 Å and a vacuum thickness of about 20 Å. The atomic structures were relaxed with the PBEsol functional and their energies were calculated with the HSE06 functional. Then, the following equation was used to calculate the surface formation energies

$$\Delta E_{surf}^f = (E_{surf} - n_{Bi}\mu_{Bi} - n_W\mu_W - n_O\mu_O)/2 \quad (5)$$

where $E_{surf}$ is the energy of slab model calculated and $n_i$ is the number of the chemical species $i$ in the slab model. Finally, from the most stable surface structure of $Bi_2WO_6$, surfaces for the quaternary oxides were made, and the band edges of bulk were aligned by using the vacuum level as a reference using the MacroDensity package.[56]

## RESULTS

**Crystal Structure.** $Bi_2WO_6$ consists of fluorite-like $(Bi_2O_2)^{2+}$ layers and perovskite-like $(WO_4)^{2-}$ layers as shown in Figure 1. Early studies of $Bi_2WO_6$ reported a range of structure types including $I4/mmm$,[25] $B2cb$,[26] and $P2_1ab$ (referred as $Pca2_1$).[24,42] There is growing consensus that this material exhibits the $P2_1ab$ structure around room temperature.[27,30−32] Our optimized structural parameters, listed in Table 1, are in good agreement with experimental results, which have reported the lattice constants of $Bi_2WO_6$ to be 5.45, 5.43, and 16.40 Å (converted from $Pca2_1$ setting).[27]

For quaternary compounds, the most stable F ion configurations within 20 calculated structures are presented in Figure 1. All of the structures were orthorhombic with the lattice constants shown in Table 1. With the exception of $Bi_2SnO_4F_2$, the volume of the unit cell decreased as the B-site cation decreased its valence (Table 1). The length of each axis depends on the F configurations and the trends can be explained by the B-site cation and F (B−F) bond length. The B−F bond length is longer than B−O, which causes the octahedra to be elongated in the F direction. This elongation decreases the volume of the octahedra and moves the B-ion closer to the center of the octahedra. Overall, in quaternary compounds, substitution of O by F ions largely changed the local structure of the perovskite-like $(BO_4)^{2-}$ layer.

Stability is an important criterion when considering photochemical or optoelectronic applications. However, it is known that ternary and quaternary compounds are more likely to be unstable compared to binary compounds because there are more competing phases.[57] Therefore, the thermodynamic stability of the compounds were assessed by whether a material will decompose to its competitive phases. All compounds were found to be stable (see the Supporting Information) with the exception of $Bi_2SnO_4F_2$. The following decomposition reaction of $Bi_2SnO_4F_2$ is exothermic

$$\Delta H = (E_{Sn_2Bi_2O_7} + E_{BiOF} + E_{BiF_3}) - 2E_{Bi_2SnO_4F_2} = -1.11\ \text{eV} \quad (6)$$

In this process, the enthalpy change $\Delta H$ was −1.11 eV, suggesting a trio of $Sn_2Bi_2O_7$, BiOF, and $BiF_3$ to be preferred over $Bi_2SnO_4F_2$ at any chemical potential range. Furthermore, using the phonopy code,[58] the first-principles phonon density of states were calculated and the absence of imaginary modes were confirmed. Because $Bi_2SnO_4F_2$ was unstable, hereafter, we will focus on four compounds, $Bi_2WO_6$, $Bi_2TaO_5F$, $Bi_2NbO_5F$, and $Bi_2TiO_4F_2$.

**Electronic Structure.** The atom-projected electronic density of states was used to investigate the contribution of each element to upper valence band and lower conduction band, as shown in Figure 2. Six inequivalent O-sites in this crystal structure were grouped according to the nearest cation. For example, in $Bi_2WO_6$, 16 O atoms were labeled $O_{Bi}$ and eight of them were labeled $O_W$ as shown in Figure 2. It should be noted that for quaternary compounds, the number of O atoms near Bi and O atoms near B-site cation varies according to the F configurations.

All four compounds, $Bi_2WO_6$, $Bi_2TaO_5F$, $Bi_2NbO_5F$, and $Bi_2TiO_4F_2$, are insulators with band gaps of 2.88, 4.16, 3.56, and 3.93 eV, respectively. Experimental studies reported that $Bi_2WO_6$ has a band gap of 2.8 eV, which is in good agreement with our calculation.[22,54,59] Judging from the small lattice constant differences, the slight overestimate of the band gap is likely to originate from the choice of the HSE06 exchange correlation functional and the absence of SOC. For the quaternary compounds, experimental studies have reported the band gaps of $Bi_2TaO_5F$, $Bi_2NbO_5F$, and $Bi_2TiO_4F_2$ to be 2.86, 2.95, and ∼3.06 eV, respectively.[34,36,41]

In addition to the band gap overestimation arising from the HSE06 functional, the smaller measured band gaps are likely to be influenced by point and extended defects. Both experimental and theoretical works reported that in $Bi_2WO_6$, oxygen vacancies are easily formed and contribute to band gap narrowing.[55,60−62] Similar characteristics are expected for quaternary compounds. Because the experimental measurements of $Bi_2TaO_5F$, $Bi_2NbO_5F$, and $Bi_2TiO_4F_2$ were performed for porous structures, abundance of defects are likely to be the reason for the smaller band gaps to be experimentally observed.

In each of the compounds studied, the upper valence band is mainly composed of the antibonding state of the O p orbitals with hybridization of the Bi s orbitals (−1.0 to 0.0 eV in Figure 2). The narrow bandwidth indicates the localized nature of these states. The density of states for $Bi_2WO_6$ is in good agreement with the previous studies.[31,61,63] In the quaternary compounds, the F levels fall deeper into the valence band



DOI: 10.1021/acs.jpcc.9b09806
J. Phys. Chem. C 2019, 123, 29155−29161

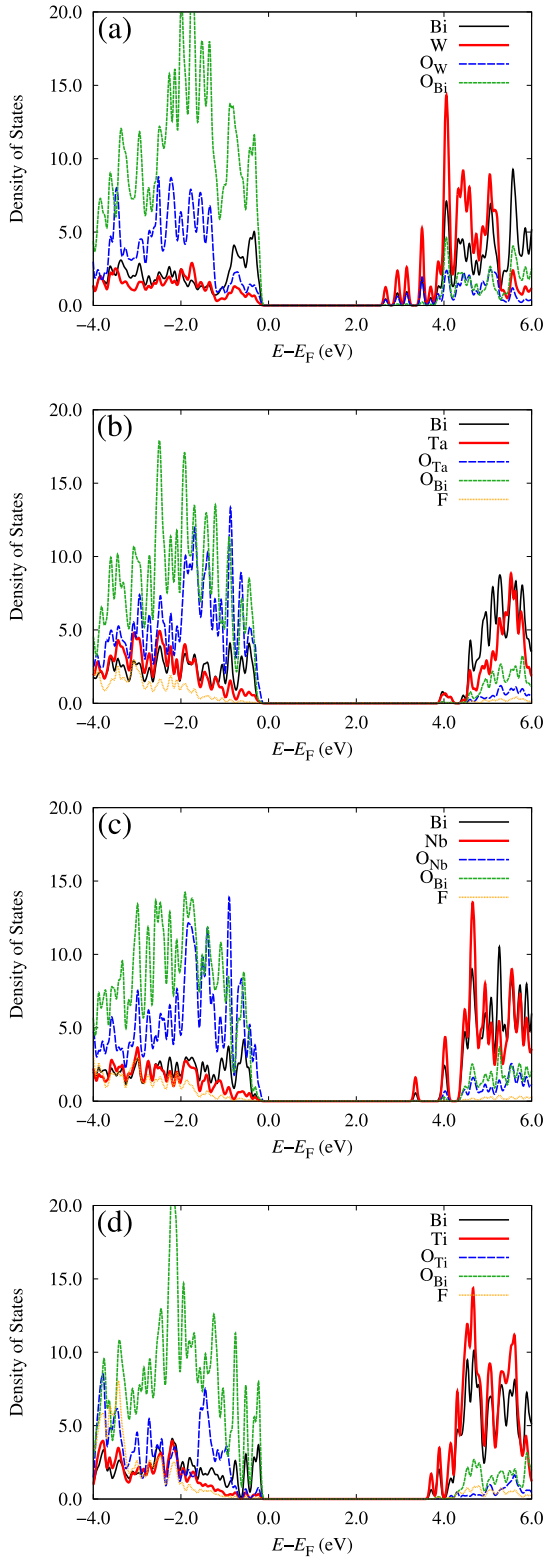


**Figure 2.** Electronic density of states projected for (a) $Bi_2WO_6$, (b) $Bi_2TaO_5F$, (c) $Bi_2NbO_5F$, and (d) $Bi_2TiO_4F_2$. $O_{Bi}$, $O_W$, $O_{Ta}$, $O_{Nb}$, and $O_{Ti}$ are oxygen atoms near Bi, W, Ta, Nb, and Ti, respectively.

(~−1.0 eV in Figure 2). This is in contrast in the case of $PbBiO_2I$, where the upper VB is mainly composed of I 5p levels. This energy level resulted in the oxidation of I to be favored over water, causing the ratio of I to decrease during oxidation reactions.[13] Therefore, having F 2p deeper in the valence band is a favorable property for avoiding photocatalyst degradation.

The lower conduction band of $Bi_2WO_6$, $Bi_2TaO_5F$, $Bi_2NbO_5F$, and $Bi_2TiO_4F_2$ is mainly composed of the $d^0$ orbitals of the B-site cations, with small contribution from Bi 6p. The metal d-peaks have a large bandwidth, suggesting spatial delocalization. This has been reported in the previous study and likely to contribute to the faster electron transport.[61]

**Lattice Polarization.** $Bi_2WO_6$ adopts a noncentrosymmetric crystal structure with results in macroscopic polarization. Within the Berry phase formalism, the polarization quanta along *a* was calculated to be 17.79−18.26 $\mu C/cm^2$ (Table 1), which are smaller than the spontaneous polarization, making it necessary to include intermediate structures for reliable predictions. The change in polarization accompanied by the lattice distortion from the reference nonpolar structure to the polar $P2_1ab$ phase of $Bi_2WO_6$ is shown in Figure 3. The resulting spontaneous polarization was 61.55 $\mu C/cm^2$. Similarly, the spontaneous polarization of quaternary compounds was calculated and is summarized in Table 1.

All of the quaternary compounds exhibit weaker polarization than $Bi_2WO_6$. As mentioned above, substitution of O by F in the perovskite-like $(BO_4)^{2-}$ layers results in a structural modification that includes a shift of the B-site cations closer to the center of their octahedra. Because the perovskite-like $(BO_4)^{2-}$ layer is largely responsible for the spontaneous polarization, this effect is the origin of the suppression. Three additional F configurations were calculated for each compounds; however, the values of the spontaneous polarization were consistently smaller than that of $Bi_2WO_6$.

**Surfaces and Band Energies.** Although analysis of the electronic structure through the bulk density of states can give us insight into the material properties, knowledge of the surface structures and band alignment is necessary to consider specific chemical reactions and device applications. Therefore, we searched for stable surface structures and analyzed the absolute band energies.

First, the chemical potentials meeting the stability condition of $Bi_2WO_6$ were obtained. Formation of $Bi_2WO_6$ was limited by the formation of $WO_3$ and $Bi_2O_3$. The possible range of $\Delta\mu_{Bi}$ was −3.7 to 0 eV, the possible range of $\Delta\mu_W$ was −9.7 to −1.5 eV, and the possible range of $\Delta\mu_O$ was −2.4 to 0 eV, as shown in Figure 4a. This phase diagram is in good agreement with previous studies.[61,64]

It has been reported that $Bi_2WO_6$ exhibits heterogeneous growth with the *a* and *b* axes showing faster growth rate, resulting in a preference for the (001) surface.[54,55] Therefore, five different (001) surfaces of $Bi_2WO_6$ were considered (Figure S5). The most stable surface for given chemical potentials was calculated and presented in Figure 4a. Within the stable region of $Bi_2WO_6$, Bi−O termination was dominant followed by Bi and W termination. The stability of Bi−O termination was also suggested in a previous computational study.[64] Furthermore, monolayer $Bi_2WO_6$ was recently synthesized and suggested to exhibit Bi−O termination.[23]

Employing the favored Bi−O terminations, the absolute electron energies were calculated and are shown in Figure 4b. The band alignment of $Bi_2WO_6$ is consistent with the behavior of experimentally measured water oxidation reactions.[65,66] The VBM of the quaternary compounds had similar levels (−6.98 to −6.93 eV). The higher VBMs of quaternary compounds compared to $Bi_2WO_6$ suggest that the effect of F is to strengthen the hybridization between Bi s and O p compared



DOI: 10.1021/acs.jpcc.9b09806
J. Phys. Chem. C 2019, 123, 29155−29161

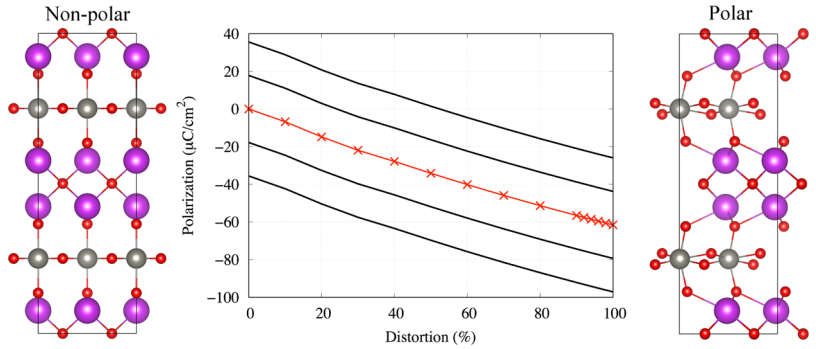


**Figure 3.** Change in electric polarization accompanied with the distortion of $WO_6$ octahedra from the reference nonpolar structure to $P2_1ab$ space group symmetry.

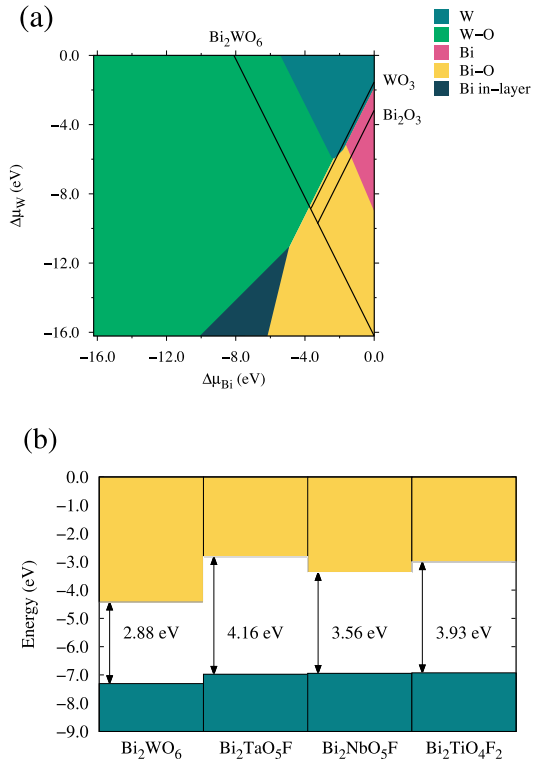


**Figure 4.** (a) Surface phase diagram drawn as a function of the chemical potentials of Bi and W. The stable area for $Bi_2WO_6$ is shown as an area surrounded by the black line labeled $Bi_2WO_6$, $WO_3$, and $Bi_2O_3$. (b) Electronic band alignment for four compounds.

to $Bi_2WO_6$. In contrast, the CBM level differed largely in each compound. Together with the result of the electronic band structures (Figure 2), the absolute position of CBM is largely dependent on the B-site cation, which suggests tunability of CBM level with substitution of B-site cations.

## CONCLUSIONS

In summary, first-principles calculations were performed to characterize $Bi_2WO_6$, $Bi_2TaO_5F$, $Bi_2NbO_5F$, $Bi_2TiO_4F_2$, and $Bi_2SnO_4F_2$. Out of four quaternary oxides, $Bi_2SnO_4F_2$ was found to be unstable, while $Bi_2TaO_5F$, $Bi_2NbO_5F$, and $Bi_2TiO_4F_2$ were stable against the decomposition reactions. Substitution of O by F ions in quaternary oxides resulted in a less polar octahedra structure, resulting in a suppressed spontaneous electric polarization. The quaternary compounds exhibit higher VBM, while the conduction band minima showed a large variation. This result suggests that the valence band can be raised by adding F and that the conduction band can be tuned by replacing the B-site cation. We demonstrated that substitution of cations and anions is effective to tune the atomic and electronic structures of $Bi_2WO_6$. The approach employed in this work is likely to contribute to understand other Bi-based mixed anion compounds.

## ASSOCIATED CONTENT

### Supporting Information

The Supporting Information is available free of charge at https://pubs.acs.org/doi/10.1021/acs.jpcc.9b09806.

Phonon density of states, decomposition reaction enthalpies, and details of surface structures (PDF)

## AUTHOR INFORMATION

### Corresponding Authors

*E-mail: k.morita18@imperial.ac.uk (K.M.).
*E-mail: a.walsh@imperial.ac.uk (A.W.).

### ORCID

Kazuki Morita: 0000-0002-2558-6963
Ji-Sang Park: 0000-0002-1374-8793
Sunghyun Kim: 0000-0001-5072-6801
Aron Walsh: 0000-0001-5460-7033

### Notes

The authors declare no competing financial interest.

## ACKNOWLEDGMENTS

This research has been partially supported by Keio University Research Grant for Young Researcher's Program, Yoshida Scholarship Foundation, Japan Student Services Organization, and Centre for Doctoral Training on Theory and Simulation of Materials at Imperial College London. Part of computation in this work has been done using the facilities of the Supercomputer Center, Institute for Solid State Physics, University of Tokyo. Some of the calculations were also carried out in the UK national Archer HPC facility, accessed through membership of the UK Materials Chemistry Consortium, which is funded by EPSRC (EP/L000202).

## REFERENCES

(1) Abe, R. Recent Progress on Photocatalytic and Photoelectrochemical Water Splitting Under Visible Light Irradiation. *J. Photochem. Photobiol., C* **2010**, *11*, 179–209.



DOI: 10.1021/acs.jpcc.9b09806
*J. Phys. Chem. C* 2019, 123, 29155–29161

(2) Hisatomi, T.; Kubota, J.; Domen, K. Recent Advances in Semiconductors for Photocatalytic and Photoelectrochemical Water Splitting. *Chem. Soc. Rev.* **2014**, *43*, 7520.
(3) Hoffmann, M. R.; Martin, S. T.; Choi, W.; Bahnemann, D. W. Environmental Applications of Semiconductor Photocatalysis. *Chem. Rev.* **1995**, *95*, 69−96.
(4) Hoel, C. A.; Mason, T. O.; Gaillard, J.-F.; Poeppelmeier, K. R. Transparent Conducting Oxides in the $ZnO$-$In_2O_3$-$SnO_2$ System. *Chem. Mater.* **2010**, *22*, 3569−3579.
(5) Scaife, D. E. Oxide semiconductors in photoelectrochemical conversion of solar energy. *Sol. Energy* **1980**, *25*, 41−54.
(6) Wang, Y.; Suzuki, H.; Xie, J.; Tomita, O.; Martin, D. J.; Higashi, M.; Kong, D.; Abe, R.; Tang, J. Mimicking Natural Photosynthesis: Solar to Renewable $H_2$ Fuel Synthesis by Z-Scheme Water Splitting Systems. *Chem. Rev.* **2018**, *118*, 5201−5241.
(7) Klein, A. Energy band alignment at interfaces of semiconducting oxides: A review of experimental determination using photoelectron spectroscopy and comparison with theoretical predictions by the electron affinity rule, charge neutrality levels, and the common anion rule. *Thin Solid Films* **2012**, *520*, 3721−3728.
(8) Paul Maruska, H.; Ghosh, A. K. Photocatalytic decomposition of water at semiconductor electrodes. *Sol. Energy* **1978**, *20*, 443−458.
(9) Ellmer, K. Past achievements and future challenges in the development of optically transparent electrodes. *Nat. Photonics* **2012**, *6*, 809.
(10) Walsh, A.; Payne, D. J.; Egdell, R. G.; Watson, G. W. Stereochemistry of Post-Transition Metal Oxides: Revision of the Classical Lone Pair Model. *Chem. Soc. Rev.* **2011**, *40*, 4455−4463.
(11) Seshadri, R.; Hill, N. A. Visualizing the Role of Bi 6s "Lone Pairs" in the Off-Center Distortion in Ferromagnetic $BiMnO_3$. *Chem. Mater.* **2001**, *13*, 2892−2899.
(12) Kageyama, H.; Hayashi, K.; Maeda, K.; Attfield, J. P.; Hiroi, Z.; Rondinelli, J. M.; Poeppelmeier, K. R. Expanding Frontiers in Materials Chemistry and Physics With Multiple Anions. *Nat. Commun.* **2018**, *9*, 772.
(13) Suzuki, H.; Kunioku, H.; Higashi, M.; Tomita, O.; Kato, D.; Kageyama, H.; Abe, R. Lead Bismuth Oxyhalides $PbBiO_2X$ (X = Cl, Br) as Visible-Light-Responsive Photocatalysts for Water Oxidation: Role of Lone-Pair Electrons in Valence Band Engineering. *Chem. Mater.* **2018**, *30*, 5862−5869.
(14) Bhatia, A.; Hautier, G.; Nilgianskul, T.; Miglio, A.; Sun, J.; Kim, H. J.; Kim, K. H.; Chen, S.; Rignanese, G.-M.; Gonze, X.; et al. High-Mobility Bismuth-Based Transparent p-Type Oxide From High-Throughput Material Screening. *Chem. Mater.* **2016**, *28*, 30−34.
(15) Fujito, H.; Kunioku, H.; Kato, D.; Suzuki, H.; Higashi, M.; Kageyama, H.; Abe, R. Layered Perovskite Oxychloride $Bi_4NbO_8Cl$: A Stable Visible Light Responsive Photocatalyst for Water Splitting. *J. Am. Chem. Soc.* **2016**, *138*, 2082−2085.
(16) Kato, D.; Hongo, K.; Maezono, R.; Higashi, M.; Kunioku, H.; Yabuuchi, M.; Suzuki, H.; Okajima, H.; Zhong, C.; Nakano, K.; et al. Valence Band Engineering of Layered Bismuth Oxyhalides Toward Stable Visible-Light Water Splitting: Madelung Site Potential Analysis. *J. Am. Chem. Soc.* **2017**, *139*, 18725−18731.
(17) Kunioku, H.; Higashi, M.; Tomita, O.; Yabuuchi, M.; Kato, D.; Fujito, H.; Kageyama, H.; Abe, R. Strong hybridization between Bi-6s and O-2p orbitals in Sillén-Aurivillius perovskite $Bi_4MO_8X$ (M = Nb, Ta; X = Cl, Br), visible light photocatalysts enabling stable water oxidation. *J. Mater. Chem. A* **2018**, *6*, 3100−3107.
(18) Benedek, N. A.; Rondinelli, J. M.; Djani, H.; Ghosez, P.; Lightfoot, P. Understanding ferroelectricity in layered perovskites: new ideas and insights from theory and experiments. *Dalton Trans.* **2015**, *44*, 10543−10558.
(19) Aurivillius, B. Mixed Bismuth Oxides With Layer Lattices. 1. The Structure Type of $CaNb_2Bi_2O_9$. *Ark. Kemi* **1950**, *1*, 463−480.
(20) Aurivillius, B. Mixed Bismuth Oxides With Layer Lattices. 2. Structure of $Bi_4Ti_3O_{12}$. *Ark. Kemi* **1950**, *1*, 499−512.
(21) Kendall, K. R.; Navas, C.; Thomas, J. K.; zur Loye, H.-C. Recent Developments in Oxide Ion Conductors: Aurivillius Phases. *Chem. Mater.* **1996**, *8*, 642−649.
(22) Kudo, A.; Hijii, S. $H_2$ or $O_2$ Evolution from Aqueous Solutions on Layered Oxide Photocatalysts Consisting of $Bi^{3+}$ with $6s^2$ Configuration and $d^0$ Transition Metal Ions. *Chem. Lett.* **1999**, *28*, 1103−1104.
(23) Zhou, Y.; Zhang, Y.; Lin, M.; Long, J.; Zhang, Z.; Lin, H.; Wu, J. C.-S.; Wang, X. Monolayered $Bi_2WO_6$ Nanosheets Mimicking Heterojunction Interface With Open Surfaces for Photocatalysis. *Nat. Commun.* **2015**, *6*, 8340.
(24) Islam, M. S.; Lazure, S.; Vannier, R.-N.; Nowogrocki, G.; Mairesse, G. Structural and Computational Studies of $Bi_2WO_6$ Based Oxygen Ion Conductors. *J. Mater. Chem.* **1998**, *8*, 655−660.
(25) Frit, B.; Mercurio, J. P. The Crystal Chemistry and Dielectric Properties of the Aurivillius Family of Complex Bismuth Oxides With Perovskite-Like Layered Structures. *J. Alloys Compd.* **1992**, *188*, 27−35.
(26) Wolfe, R. W.; Newnahm, R. E.; Kay, M. I. Crystal Structure of $Bi_2WO_6$. *Solid State Commun.* **1969**, *7*, 1797−1801.
(27) Yoneda, Y.; Kohara, S.; Takeda, H.; Tsurumi, T. Local Structure Analysis of $Bi_2WO_6$. *Jpn. J. Appl. Phys.* **2012**, *51*, 09LE06.
(28) Djani, H.; Hermet, P.; Ghosez, P. First-Principles Characterization of the P21abFerroelectric Phase of Aurivillius $Bi_2WO_6$. *J. Phys. Chem. C* **2014**, *118*, 13514−13524.
(29) Okudera, H.; Sakai, Y.; Yamagata, K.; Takeda, H. Structure of Russellite ($Bi_2WO_6$): Origin of Ferroelectricity and the Effect of the Stereoactive Lone Electron Pair on the Structure. *Acta Crystallogr., Sect. B: Struct. Sci., Cryst. Eng. Mater.* **2018**, *74*, 295.
(30) Knight, K. S. The Crystal Structure of Ferroelectric $Bi_2WO_6$ at 961 K. *Ferroelectrics* **1993**, *150*, 319−330.
(31) Mohn, C. E.; Stølen, S. Influence of the Stereochemically Active Bismuth Lone Pair Structure on Ferroelectricity and Photocalytic Activity of Aurivillius Phase $Bi_2WO_6$. *Phys. Rev. B: Condens. Matter Mater. Phys.* **2011**, *83*, 014103.
(32) McDowell, N. A.; Knight, K. S.; Lightfoot, P. Unusual High-Temperature Structural Behaviour in Ferroelectric $Bi_2WO_6$. *Chem.—Eur. J.* **2006**, *12*, 1493−1499.
(33) Djani, H.; Bousquet, E.; Kellou, A.; Ghosez, P. First-Principles Study of the Ferroelectric Aurivillius Phase $Bi_2WO_6$. *Phys. Rev. B: Condens. Matter Mater. Phys.* **2012**, *86*, 054107.
(34) Jiang, B.; Zhang, P.; Zhang, Y.; Wu, L.; Li, H.; Zhang, D.; Li, G. Self-Assembled 3D Architectures of $Bi_2TiO_4F_2$ as a New Durable Visible-Light Photocatalyst. *Nanoscale* **2012**, *4*, 455−460.
(35) Li, G.; Jiang, B.; Li, X.; Lian, Z.; Xiao, S.; Zhu, J.; Zhang, D.; Li, H. $C_{60}$/$Bi_2TiO_4F_2$ Heterojunction Photocatalysts With Enhanced Visible-Light Activity for Environmental Remediation. *ACS Appl. Mater. Interfaces* **2013**, *5*, 7190−7197.
(36) Lei, S.; Cheng, D.; Gao, X.; Fei, L.; Lu, W.; Zhou, J.; Xiao, Y.; Cheng, B.; Wang, Y.; Huang, H. A new low-temperature solution route to Aurivillius-type layered oxyfluoride perovskites $Bi_2MO_5F$ (M = Nb, Ta) as photocatalysts. *Appl. Catal., B* **2017**, *205*, 112−120.
(37) Medvedeva, N. I.; Gubanov, V. A. Electronic Structure and Properties of Aurivillius Phases. *J. Struct. Chem.* **1996**, *37*, 409−416.
(38) Kodama, H.; Izumi, F.; Watanabe, A. New Members of a Family of Layered Bismuth Compounds. *J. Solid State Chem.* **1981**, *36*, 349−355.
(39) McCabe, E. E.; Jones, I. P.; Zhang, D.; Hyatt, N. C.; Greaves, C. Crystal structure and electrical characterisation of $Bi_2NbO_5F$: an Aurivillius oxide fluoride of $Bi_2NbO_5$ F: An Aurivillius Oxide Fluoride. *J. Mater. Chem.* **2007**, *17*, 1193−1200.
(40) Needs, R. L.; Sandra, E.; Weller, M. T.; Cherryman, J. C.; Harris, R. K. The Structure and Oxide/Fluoride Ordering of the Ferroelectrics $Bi_2TiO_4F_2$ and $Bi_2NbO_5$ F. *J. Mater. Chem.* **2005**, *15*, 2399−2407.
(41) Lei, S.; Gao, X.; Cheng, D.; Fei, L.; Lu, W.; Zhou, J.; Xiao, Y.; Cheng, B.; Wang, Y.; Huang, H. A Hierarchically Porous Hollow Structure of Layered Bi2TiO4F2 for Efficient Photocatalysis. *Eur. J. Inorg. Chem.* **2017**, *2017*, 1892−1899.
(42) Knight, K. S. The Crystal Structure of Russellite; A Re-Determination Using Neutron Powder Diffraction of Synthetic $B_2WO_6$. *Mineral. Mag.* **1992**, *56*, 399−409.


DOI: 10.1021/acs.jpcc.9b09806
J. Phys. Chem. C 2019, 123, 29155−29161

(43) Grau-Crespo, R.; Hamad, S.; Catlow, C. R. A.; de leeuw, N. H. Symmetry-Adapted Configurational Modelling of Fractional Site Occupancy in Solids. *J. Phys.: Condens. Matter* **2007**, *19*, 256201.
(44) Blöchl, P. E. Projector Augmented-Wave Method. *Phys. Rev. B: Condens. Matter Mater. Phys.* **1994**, *50*, 17953.
(45) Kresse, G.; Furthmüller, J. Efficiency of Ab-Initio Total Energy Calculations for Metals and Semiconductors Using a Plane-Wave Basis Set. *Comput. Mater. Sci.* **1996**, *6*, 15−50.
(46) Kresse, G.; Furthmüller, J. Efficient iterative schemes for ab initio total-energy calculations using a plane-wave basis set. *Phys. Rev. B: Condens. Matter Mater. Phys.* **1996**, *54*, 11169.
(47) Momma, K.; Izumi, F. VESTA 3 for three-dimensional visualization of crystal, volumetric and morphology data. *J. Appl. Crystallogr.* **2011**, *44*, 1272−1276.
(48) Heyd, J.; Scuseria, G. E.; Ernzerhof, M. Hybrid Functionals Based on a Screened Coulomb Potential. *J. Chem. Phys.* **2003**, *118*, 8207−8215.
(49) Perdew, J. P.; Ruzsinszky, A.; Csonka, G. I.; Vydrov, O. a.; Scuseria, G. E.; Constantin, L. a.; Zhou, X.; Burke, K. Restoring the Density-Gradient Expansion for Exchange in Solids and Surfaces. *Phys. Rev. Lett.* **2008**, *100*, 136406.
(50) Yang, J.; Dolg, M. First-Principles Electronic Structure Study of the Monoclinic Crystal Bismuth Triborate $BiB_3O_6$. *J. Phys. Chem. B* **2006**, *110*, 19254−19263.
(51) Sun, Y.-Y.; Shi, J.; Lian, J.; Gao, W.; Agiorgousis, M. L.; Zhang, P.; Zhang, S. Discovering lead-free perovskite solar materials with a split-anion approach. *Nanoscale* **2016**, *8*, 6284−6289.
(52) Resta, R. Theory of the Electric Polarization in Crystals. *Ferroelectrics* **1992**, *136*, 51−55.
(53) King-Smith, R. D.; Vanderbilt, D. Theory of Polarization of Crystalline Solids. *Phys. Rev. B: Condens. Matter Mater. Phys.* **1993**, *47*, 1651.
(54) Saison, T.; Chemin, N.; Chanéac, C.; Durupthy, O.; Ruaux, V.; Mariey, L.; Maugé, F.; Beaunier, P.; Jolivet, J.-P. $Bi_2O_3$, $BiVO_4$, and $Bi_2WO_6$: Impact of Surface Properties on Photocatalytic Activity Under Visible Light. *J. Phys. Chem. C* **2011**, *115*, 5657−5666.
(55) Liu, X.; Long, P.; Sun, Z.; Yi, Z. Optical, Electrical and Photoelectric Properties of Layered-Perovskite Ferroelectric $Bi_2WO_6$ Crystals. *J. Mater. Chem. C* **2016**, *4*, 7563−7570.
(56) Butler, K. T.; Hendon, C. H.; Walsh, A. Electronic Chemical Potentials of Porous Metal-Organic Frameworks. *J. Am. Chem. Soc.* **2014**, *136*, 2703−2706.
(57) Davies, D. W.; Butler, K. T.; Walsh, A. Data-Driven Discovery of Photoactive Quaternary Oxides Using First-Principles Machine Learning. *Chem. Mater.* **2019**, *31*, 7221−7230.
(58) Togo, A.; Tanaka, I. First principles phonon calculations in materials science. *Scr. Mater.* **2015**, *108*, 1−5.
(59) Ng, C.; Iwase, A.; Ng, Y. H.; Amal, R. Transforming Anodized $WO_3$ Films Into Visible-Light-Active $Bi_2WO_6$ Photoelectrodes by Hydrothermal Treatment. *J. Phys. Chem. Lett.* **2012**, *3*, 913−918.
(60) Utkin, V. I.; Roginskaya, Y. E.; Voronkova, V. I.; Yanovskii, V. K.; Sh. Galyamov, B.; Venevtsev, Y. N. Dielectric Properties, Electrical Conductivity, and Relaxation Phenomena in Ferroelectric $Bi_2WO_6$. *Phys. Status Solidi A* **1980**, *59*, 75−82.
(61) Jing, T.; Dai, Y.; Wei, W.; Ma, X.; Huang, B. Near-infrared photocatalytic activity induced by intrinsic defects in $Bi_2MO_6$ (M = W, Mo). *Phys. Chem. Chem. Phys.* **2014**, *16*, 18596−18604.
(62) Zhang, S.; Pu, W.; Du, H.; Wang, Y.; Yang, C.; Gong, J. Facile synthesis of Pt assisted Bi-$Bi_2WO_{6-x}$ with oxygen vacancies for the improved photocatalytic activity under visible light. *Appl. Surf. Sci.* **2018**, *459*, 363−375.
(63) Li, M.; Dai, Y.; Wei, W.; Huang, B. A Comprehensive Study of Electronic and Photocatalytic Properties in Monolayer, Double-Layer and Bulk $Bi_2WO_6$. *Phys. Chem. Chem. Phys.* **2018**, *20*, 9221−9227.
(64) Ren, F.; Zhang, J.; Wang, Y.; Yao, W. A Graphene-Coupled $Bi_2WO_6$ Nanocomposite With Enhanced Photocatalytic Performance: A First-Principles Study. *Phys. Chem. Chem. Phys.* **2016**, *18*, 14113−14121.
(65) Hill, J. C.; Choi, K.-S. Synthesis and Characterization of High Surface Area $CuWO_4$ and $Bi_2WO_6$ Electrodes for Use as Photoanodes for Solar Water Oxidation. *J. Mater. Chem. A* **2013**, *1*, 5006−5014.
(66) Kang, D.; Park, Y.; Hill, J. C.; Choi, K.-S. Preparation of Bi-Based Ternary Oxide Photoanodes $BiVO_4$, $Bi_2WO_6$, and $Bi_2Mo_3O_{12}$ Using Dendritic Bi Metal Electrodes. *J. Phys. Chem. Lett.* **2014**, *5*, 2994−2999.


DOI: 10.1021/acs.jpcc.9b09806
*J. Phys. Chem. C* 2019, 123, 29155−29161